Fuel Processing Technology 173 (2018) 173–181

Contents lists available at ScienceDirect

Fuel Processing Technology

journal homepage: www.elsevier.com/locate/fuproc

Kinetics of the hydrogenation of CO_2 to methanol at atmospheric pressure using a Pd-Cu-Zn/SiC catalyst

J. Díez-Ramírez, J.A. Díaz*, F. Dorado, P. Sánchez

Departamento de Ingeniería Química, Facultad de Ciencias y Tecnologías Químicas, Universidad de Castilla – La Mancha, Avenida Camilo José Cela 12, 13071 Ciudad Real, Spain

ARTICLE INFO

Keywords:
CO_2 hydrogenation
Methanol
Langmuir–Hinshelwood
Kinetic

ABSTRACT

The kinetics of the hydrogenation of CO_2 to methanol (MeOH) at atmospheric pressure using a Pd-Cu-Zn/SiC catalyst has been analyzed. An initial sensitivity study was performed in order to evaluate the effect of reaction conditions (temperature, CO_2/H_2 ratio and the presence of products in the feed stream) on the catalytic performance. The results of this study were used to develop three Langmuir–Hinshelwood kinetic models in which the adsorption term was modified (competitive vs two-site vs three-site adsorption mechanism). All of the kinetic models predicted the experimental results well and the corresponding parameters were statistically meaningful. Model discrimination revealed that the three-site adsorption mechanism led to the lowest residual sum of squares and was the only one that met all of the parameter constraints. The quality of this model was evaluated by comparing the results of additional experiments with the predicted values. The three-site adsorption mechanism agreed with the catalytic observations reported previously, where it was observed that, in the presence of a Pd-Cu-Zn/SiC catalyst, the synthesis of MeOH by hydrogenation of CO_2 took place on PdZn active sites, whereas the Reverse Water Gas Shift (RWGS), which led to CO, was catalyzed by PdCu sites. The H_2 dissociative adsorption was believed to take place on ZnO.

1. Introduction

Carbon dioxide is considered to be the main contributor to global warming and it is therefore one of the most harmful pollutants to the ecosystem [1]. At the same time, it is one of the most promising sources of carbon to produce other compounds such as hydrocarbons, alcohols, and aldehydes, among others [2]. In this regard, the scientific community is working on the development of processes to transform the CO_2 pollution problem into an opportunity to obtain valuable products.

The hydrogenation of carbon dioxide to methanol (MeOH, Eq. (1)) is one of the ways in which this pollutant can be valorized [3]. MeOH is frequently used as a solvent and a feedstock to produce chemicals. MeOH could be used as a fuel in the energy distribution infrastructure that currently exists, in a direct MeOH fuel cell [4], or it could be blended with gasoline [5].

$$CO_2 + 3H_2 \leftrightarrows CH_3OH + H_2O \quad \Delta H_{25°C} = -49.5\ kJ{\cdot}mol^{-1} \tag{1}$$

The reverse water gas shift reaction (RWGS, Eq. (2)), which also participates in the hydrogenation process, leads to carbon monoxide and this is considered to be an undesirable by-product. In this sense, the use of catalysts in order to improve the MeOH selectivity and the CO_2 conversion is crucial.

$$CO_2 + H_2 \leftrightarrows CO + H_2O \quad \Delta H_{25°C} = 41\ kJ{\cdot}mol^{-1} \tag{2}$$

Up to date, the vast majority of the research concerning this reaction is focused on the development of novel catalysts. In this regard, Wisaijorn et al. [6] modified copper-based catalysts by oyster shell-derived calcium oxide, and concluded that this material can prevent sintering of Cu particles and promoted the adsorption of CO_2. Zhao et al. [7] used Atomic Layer Deposition (ALD) to deposite Ni particles over Cu/Al_2O_3 catalysts, which led to the formation of CuNi alloys which were active in this reaction. Another example is the work reported by An et al. [8], who supported in situ Cu/ZnO_x nanoparticles in Metal-Organic Frameworks (MOFs), at a reaction temperature of 250 °C under hydrogen atmosphere. As a result, they obtained ultra-small Cu/ZnOx nanoparticles which showed high catalytic activity and selectivity to methanol.

Several different kinetic models for the synthesis of MeOH by CO_2 hydrogenation have been reported in the literature to date. Skrzypek et al. [10] proposed a Langmuir–Hinshelwood (LH) kinetic model that considers the competitive adsorption of species. Graaf et al. [11] supposed a dual-site mechanism in which H_2 and H_2O are adsorbed by ZnO

* Corresponding author.
E-mail address: JoseAntonio.Diaz@uclm.es (J.A. Díaz).

https://doi.org/10.1016/j.fuproc.2018.01.024
Received 29 November 2017; Received in revised form 18 January 2018; Accepted 28 January 2018
Available online 05 February 2018
0378-3820/

Nomenclature

C_S	CO_2 surface concentration
D_{eff}	Catalyst effective diffusivity [m^2/s]
D_x	Adsorption terms
Ea_x	Activation energy [kJ/mol]
F_{Pi}	Species molar flow
ΔH	Heat of reaction [kJ/mol]
ΔH^0_{ads}	Enthalpy of adsorption [kJ/mol]
k'_x	Reaction rate constant
$K_{i,S}$	dsorption equilibrium constant of species i in the active site s
Keq_x	Equilibrium constant of reaction rate
n	Number of data
$N_{W\text{-}P}$	Weisz–Prater number
p	Number of parameters
P_i	Partial pressure of the component i [bar]
R	Gas constant [R = 8.314 J/mol·K]
r	CO_2 initial conversion rate [%]
r_x	Reaction rate [mol_i/g_{cat}·min]
r^2	Regression coefficient
s_1	PdZn active site
s_2	ZnO active site
s_3	PdCu active site
s_i	Residual ($P_{iexp} - P_{itheo}$)
ΔS^0_{ads}	Entropy of adsorption [kJ/mol·K]
T	Temperature [K]
W	Catalyst mass [g]
w	Weighting factor
WRSS	Weighted Residual Sum of Squares

Greek Letters

ρ_c	Catalyst density [kg/m^3]

Subscripts

exp	Experimental data
i	Species
theo	Theoretical data
x	Reactions (MeOH-CO_2, RWGS, MeOH-CO)

active sites and carbonaceous species by metallic copper sites. This model has also been proposed by several authors [13]. Finally, Park et al. [12] supposed a three-site adsorption mechanism, where the adsorption of hydrogen occurs on ZnO whereas CO and CO_2 are adsorbed on Cu^{1+} and Cu^0, respectively. The vast majority of the kinetic models, such as those outlined above, have been developed using commercial $Cu/ZnO/Al_2O_3$ catalysts and only some few ones have been developed with other catalyst configurations, such as $Cu/ZnO/Al_2O_3/ZrO_2$ [13] or Pd-Ga_2O_3/Silica [14]. Moreover, only Chiavassa et al. [14] studied exclusively the hydrogenation of CO_2.

In our previous work [15], we optimized a PdCuZn/SiC catalyst by modifying the Pd/Cu ratio. Taking into account the secondary role of Zn in this reaction (hydrogen adsorption and dissociation), a highly enough proportion of this metal was deposited in each catalyst. On the other hand, as Pd and Cu are reported to be active phases in this reaction, the proportion of these metals was modified in a broad range in order to get an optimal trimetallic formulation, which was more active and selective than the corresponding bimetallic ones. By doing this, it was possible to tailor the formation of PdZn and PdCu nanoparticles which catalyzed the synthesis of methanol (Eq. (1)) and inhibited the RWGS (Eq. (2)), respectively, thus obtaining an optimum trimetallic formulation (see below) that maximizes the methanol formation rate. This catalyst formulation will be used in the later stage of the project, in which an electrocatalytic reactor, operating at atmospheric pressure, will be developed for the synthesis of methanol with a feed of CO_2 and H_2O. This electrocatalytic reactor will have two chambers separated by a co-ionic ceramic conductor. Water splitting will take place in the anodic chamber, whereas methanol synthesis will occurred in the cathodic one. By application of an electrical current, the system will act as an electrochemical hydrogen/oxygen pump (H^+ will be pumped to the cathode and O^{2-} will be pumped away from the cathode). Under this mode of operation, controlled H^+ fluxes to the cathodic catalyst are expected to create high surface hydrogen activities, which in turn will force equilibrium to the production of methanol, bypassing the conventional necessity for high pressure. At the same time O^{2-} pumping from the cathode is expected to activate the C═O bond of the adsorbed CO_X species, so that methanol synthesis will be accelerated. This way, it is expected to overcome the two main drawbacks of the so-called conventional catalytic operation: the need of high pressure operation and fossil fuel-derived hydrogen gas.

The aim of the work described here was to perform the kinetic analysis and modeling for the synthesis of MeOH by CO_2 hydrogenation at atmospheric pressure, using the PdCuZn/SiC catalyst above mentioned, as a prior step to the development of the electrocatalytic reactor. Firstly, a sensitivity study was carried out by varying the composition of the feed stream and the temperature. Secondly, three different Langmuir-Hinshelwood kinetic models were developed as a function of the adsorption mechanism. Finally, the proposed models were compared and a proper model discrimination was carried out.

2. Experimental

2.1. Catalyst preparation and characterization

A PdCuZn/SiC catalyst with a molar percentage of 37.5% Pd, 12.5% Cu and 50% Zn (0.01 total moles) was used in this work. All of the information related to the preparation and characterization (N_2 Adsorption/Desorption, XRD, TPR, TEM, XPS) was published in a previous paper by our group [15]. This tri-metallic catalyst showed better catalytic performance in the hydrogenation of CO_2 to MeOH than the bi-metallic PdZn/SiC and CuZn/SiC counterparts.

2.2. Catalyst activity measurements

Catalytic tests were carried out in a tubular quartz reactor (45 cm length and 1 cm diameter). The catalyst, which consisted of pellets that were 3 mm in length and 1 mm in diameter, was placed on a fritted quartz plate located at the end of the reactor. The amount of catalyst used in the experiments was 0.8 g.

The temperature of the catalyst was measured with a K-type thermocouple (Thermocoax) placed inside the inner quartz tube. The entire reactor was placed in a furnace (Lenton) equipped with a temperature-programed system. Reaction gases were Praxair certified standards of CO_2 (99.999% purity), H_2 (99.999% purity), N_2 (99.999% purity), CH_3OH (0.5% diluted in N_2) and CO (99.999% purity). The gas flows were controlled by a set of calibrated mass flowmeters (Brooks 5850 E and 5850 S).

The hydrogenation of CO_2 was carried out at atmospheric pressure. The feed composition was different in each experiment, keeping the total flow at 110 Nml·min^{-1}, using N_2 as a balance (GHSV = 6600 h^{-1}). The specific compositions used in all experiments are listed in Table 1. Experiments with CO_2 and H_2 in the feed stream were carried out at 473, 498, 523 and 548 K. The rest of the experiments, in which CO or MeOH were added to the feed, were evaluated at

Table 1
List of experiments (species volume flow in Nml·min^{-1}).

Experiment	CO_2/H_2 ratio	CO_2	H_2	CH_3OH	CO	N_2
1	0.30	25	82.5	0	0	2.5
2	0.30	25	82.5	0	0.5	2
3	0.33	25	75	3	0	7
4	0.33	25	75	0	0.5	9.5
5	0.33	25	75	0	0	10
6	0.19	17.5	90	0	0.5	2
7	0.19	17.5	90	0	0	2.5
8	0.21	17.5	82.5	3	0	7
9	0.21	17.5	82.5	0	0.5	9.5
10	0.21	17.5	82.5	0	0	10
11	0.23	17.5	75	3	0	14.5
12	0.23	17.5	75	0	0.5	17
13	0.23	17.5	75	0	0	17.5
14	0.11	10	90	3	0	7
15	0.11	10	90	0	0.5	9.5
16	0.11	10	90	0	0	10
17	0.12	10	82.5	3	0	14.5
18	0.12	10	82.5	0	0.5	17
19	0.12	10	82.5	0	0	17.5
20	0.13	10	75	3	0	22
Extra experiments (for comparative purposes)						
21	0.25	20	80	0	0	10
22	0.15	13	85	0	0	12

498 and 523 K.

Gas effluents were monitored with a micro gas chromatograph (Varian CP-4900) fitted with a PoraPLOT Q column and a molecular sieve column, each of which was connected to a thermal conductivity detector (TCD).

Catalytic parameters were calculated as follows (Eqs. (3)–(5)):

$$\text{Formation rate}_i\ (\mu\text{mol}\cdot\text{min}^{-1}\cdot\text{g}^{-1}) = \frac{F_i - F_i^0}{W} \tag{3}$$

$$\text{Selectivity}_i\ (\%) = \frac{F_i - F_i^0}{F_{CO_2}^0 - F_{CO_2}} \times 100 \tag{4}$$

$$CO_2\text{conversion}\ (\%) = \frac{F_{CO_2}^0 - F_{CO_2}}{F_{CO_2}^0} \times 100 \tag{5}$$

where F_i and F°_i represent the outlet and inlet molar flow (μmol·min^{-1}) of the i component (CH_3OH or CO) and W refers to the catalyst mass (g).

3. Results and discussion

3.1. Catalyst activity

3.1.1. Influence of the temperature

The catalytic results for all the experiments in which only CO_2 and H_2 were fed are represented in Fig. 1. The results are arranged from highest to lowest CO_2/H_2 ratio in the feed. The MeOH synthesis reaction is exothermic (Eq. (1)) and, as a consequence, MeOH production is favored at low temperatures, as can be seen in the selectivity graph (Fig. 1b; note that the temperature axis is in reverse order). However, due to the high stability of the CO_2 molecule, high temperatures are required to activate it (Fig. 1a). For this reason, the methanol formation rate curve is bell-shaped with a maximum at 523 K (Fig. 1c). The MeOH selectivity decreased at higher temperatures as a consequence of the formation of CO (Fig. 1d), the formation of which by the RWGS is favored at high temperatures (Eq. (2)).

3.1.2. Influence of the CO_2/H_2 ratio

The influence of the CO_2/H_2 ratio on the CO_2 conversion is represented in Fig. 1a. Three different regions, which are related to CO_2 volume flows of 25 Nml·min^{-1} (Exp. 5 and 1), 17.5 Nml·min^{-1} (Exp. 13, 10 and 7) and 10 Nml·min^{-1} (Exp. 19 and 16), can be identified. In each region, the variation of H_2 volume flow did not affect CO_2 conversion. On the other hand, the differences in CO_2 conversion between

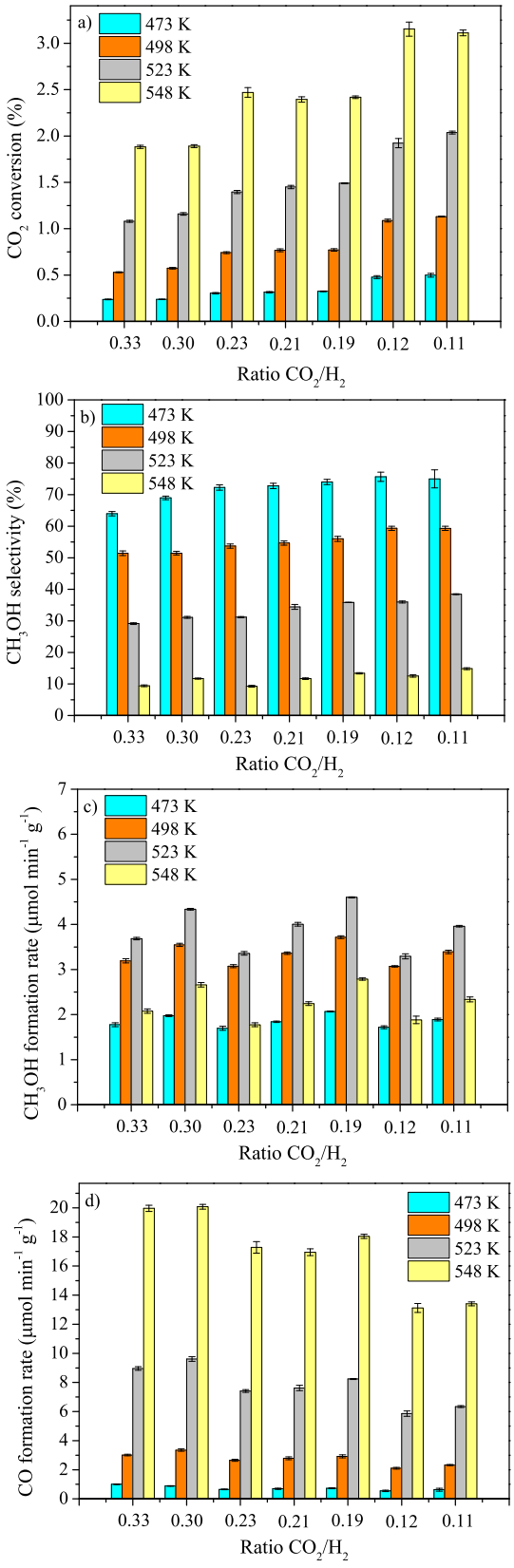

Fig. 1. Catalytic results of all experiments with only CO_2 and H_2 in the feed: a) CO_2 conversion, b) CH_3OH selectivity, c) CH_3OH formation rate and d) CO formation rate.

the regions are significant: the lower the CO_2 volume flow in the feed stream, the higher the CO_2 conversion, which can be explained considering thermodynamics of reaction (1): by using excess H_2 the equilibrium is pushed to the products side.

The influence of the CO_2/H_2 ratio on methanol selectivity is shown in Fig. 1b. In general, higher MeOH selectivity (Fig. 1b) and lower CO production (Fig. 1d) were obtained at lower CO_2/H_2 ratios, as also observed in a previous study [16]. For the same CO_2 volume flow in the regions mentioned above, a higher H_2 volume flow gives rise to higher methanol selectivity. This trend is also consistent with Fig. 1c: the highest methanol formation rates were obtained in the experiments in which the highest volume flow of H_2 was used at constant CO_2 values. According to stoichiometry of reactions (1) and (2), a higher hydrogen concentration favored methanol formation against RWGS.

The selection of the appropriate CO_2/H_2 ratio to carry out the CO_2 hydrogenation reaction depends on the requirements of the system in which the MeOH synthesis is carried out. For instance, if high conversions are needed, it would be better to work at high hydrogen concentrations, which is required in electrochemical reactors where conversion is usually poor [16]. A decrease in the CO_2/H_2 ratio leads to an increase in the CO_2 conversion and MeOH selectivity. It should be considered that the use of hydrogen limits the economic benefits of the methanol production [3,5] and, given this limitation, higher ratios (e.g. 1/3, 1/4) are used [17–19].

3.1.3. Influence of the presence of CO and CH_3OH in the feed

Experiments with small amounts of MeOH and CO in the feed stream were carried out in order to evaluate the role of the products in the reaction mechanism. The catalytic results of the experiments with only CO_2 and H_2 in the feed stream at 498 and 523 K are represented in Fig. 2 along with those in which CO or MeOH was also included. Although marked differences in the results are not observed, some interesting points should be highlighted. As expected, the presence of both products led to a decrease in the CO_2 conversion (Fig. 2a) since they shifted the equilibrium reactions (Eqs. (1) and (2)) to the left-hand side. Regarding methanol selectivity (Fig. 2b), a general decrease in the experiments with CO and MeOH was also observed – except for experiments 12 and 18, which showed a slight increase. Finally, the effect on the corresponding formation rates (Fig. 2c and d) warrants a special mention. On the one hand, the aforementioned equilibrium shift explained the fact that, when MeOH or CO were introduced in the feed, the corresponding formation rates decreased. On the other hand, the addition of MeOH did not practically affect the CO formation rate, whereas the addition of CO led to a decrease in the formation of MeOH. This behavior can be explained by considering the species adsorption equilibria. In agreement with the results shown in Fig. 2c and d, MeOH adsorption on the catalyst active sites was practically negligible whereas CO adsorption was considerable, since it also had a negative effect on the MeOH formation rate. This adsorption effect was confirmed by the fact that, in experiments with CO, higher reaction temperatures led to a less marked decrease in the MeOH formation rate, as a consequence of the weaker CO adsorption at higher reaction temperatures.

3.2. Kinetic model

3.2.1. Evaluation of diffusion limitations

Potential external diffusion limitations were evaluated using a semi-empirical method based on the following criterion:

$$\left|\frac{P_i - P_{is}}{P_i}\right| < 0.1 \tag{6}$$

where P_i is the partial pressure of the component i in the feed and P_{is} is the corresponding surface concentration. P_{is} was calculated using an iterative procedure proposed by Froment and Bischoff [20]: firstly, P_{is} was supposed to be equal to P_i, then this value was used to estimate the mass transfer coefficient (k_g), which finally was used to calculate the new value of P_{is}. The procedure was repeated until no change of P_{is} was observed. As an example, the value obtained in Eq. (6) using the results for the CO_2 conversion rate at 523 K was 0.0001, which means that external diffusion limitations could be ruled out.

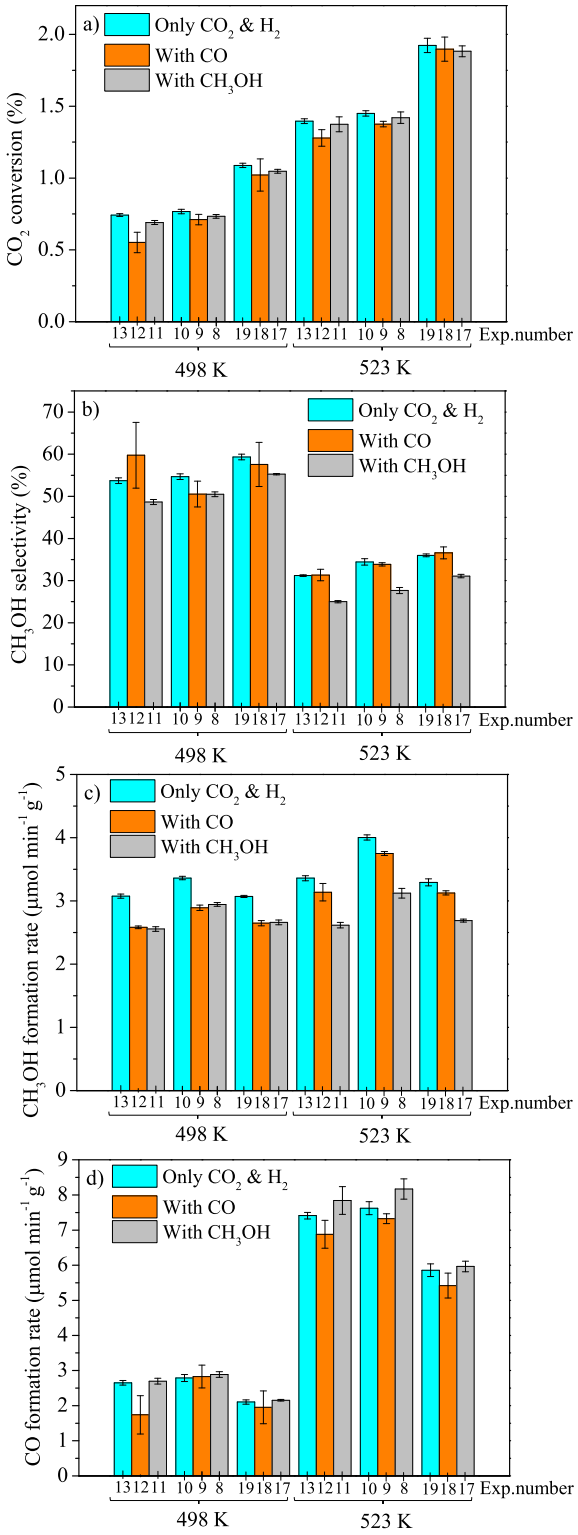

Fig. 2. Influence of the presence of CO and CH_3OH in the feed on the catalytic results: a) CO_2 conversion, b) CH_3OH selectivity, c) CH_3OH formation rate and d) CO formation rate.

Regarding internal diffusion limitations, the Weisz–Prater criterion was used. The Weisz–Prater number, $N_{W\text{-}P}$, should meet the following inequation:

$$N_{W-P} = \frac{r \cdot \rho_C \cdot R_C^2}{C_S \cdot D_{eff}} \leq 1 \quad (7)$$

where r is the CO_2 initial conversion rate, ρ_c the catalyst density (800 kg/m^3), R_C the catalyst pellet volume/surface area ratio, C_S the CO_2 surface concentration (equal to the bulk concentration since external diffusion limitations were not observed) and D_{eff} the catalyst effective diffusivity. As an example, the results for the reaction at 523 K led to an $N_{W\text{-}P}$ value of $7{\cdot}10^{-16}$, which shows that internal diffusion limitations can be ruled out.

Finally, a stability test was carried out in order to evaluate potential catalyst deactivation. In this test four reaction cycles between 423 and 523 K were performed and the results were compared, using a mixture of 100 Nml·min^{-1} of CO_2 and H_2 with a volume ratio 1/9 (Fig. 3). Each temperature was kept until steady state was attained. Once a cycle was completed, the catalyst was kept under N_2 atmosphere at 423 K overnight, prior to carry out the next one. As can be observed, all cycles overlapped and this indicates that the catalyst was stable under the conditions studied in this work and catalyst deactivation was not included in the kinetic models proposed thereafter.

3.2.2. Kinetic analysis

Firstly, it was evaluated whether the adsorption, chemical surface reaction or desorption phenomena was the rate determining step (*r.d.s.)* of the process. This was achieved by carrying out reactions with different CO_2/H_2 ratios (*v*/v) and evaluating the influence on the initial reaction rate (Fig. 4). It was observed that the reaction rate reached a maximum at a $CO_2/H_2 \approx 0.36$ and then showed a slight decrease. According to the literature [21], only those reactions in which the chemical reaction is the *r.d.s.* can show this profile, where the reactants ratio play a crucial role and a maximum is observed. If other phenomenon (adsorption or desorption) had been the *r.d.s.*, this parameter would have been irrelevant and a straight line would have been observed.

The synthesis of MeOH by CO_2 hydrogenation involves three main reactions: Eq. (1), Eq. (2) and CO hydrogenation (Eq. (8)):

$$CO + 2H_2 \leftrightarrows CH_3OH \quad \Delta H_{25°C} = -90.5\ kJ{\cdot}mol^{-1} \quad (8)$$

It was initially assumed that all reactions occur simultaneously on the surface of the catalyst. The mechanism reported by Lim et al. [13] was used to propose the reaction rate equations (Table 2), with reactions marked with *(r.d.s.)* being the corresponding rate determining steps. Regarding the hydrogenation of CO_2, it has also been reported [22] that the hydrogenation of formate is the most likely *r.d.s.* Therefore, the following reaction rate equations were proposed:

CO_2 hydrogenation: $r_{MeOH-CO_2}$

$$= \frac{k'_{MeOH-CO_2} \cdot K_{CO_2,s1} \cdot K_{H_2,s2} \cdot \frac{\left(P_{CO_2} \cdot P_{H_2}^3 - \frac{P_{MeOH} \cdot P_{H_2O}}{K_{eqMeOH-CO_2}}\right)}{P_{H_2}^2}}{D_{MeOH-CO_2}} \quad (9)$$

Reverse WGS: r_{RWGS}

$$= \frac{k'_{RWGS} \cdot K_{CO_2,s3} \cdot K_{H_2,s2}^{0.5} \cdot \frac{\left(P_{CO_2} \cdot P_{H_2} - \frac{P_{CO} \cdot P_{H_2O}}{K_{eqRWGS}}\right)}{P_{H_2}^{0.5}}}{D_{RWGS}} \quad (10)$$

CO hydrogenation: $r_{MeOH-CO}$

$$= \frac{k'_{MeOH-CO} \cdot K_{CO,s1} \cdot K_{H_2,s2} \cdot \frac{\left(P_{CO_2} \cdot P_{H_2}^3 - \frac{P_{MeOH} \cdot P_{H_2O}}{K_{eqMeOH-CO}}\right)}{P_{H_2}^2}}{D_{MeOH-CO}} \quad (11)$$

In this work, three different Langmuir–Hinshelwood models were proposed: in the first one, reactants were supposed to adsorb competitively on the catalyst active sites. The second one considered two adsorption sites: Pd-based nanoparticles that adsorbed carbonaceous species (CO, CH_3OH and CO_2), and ZnO, on which H_2 and H_2O were adsorbed. Finally, a three-site kinetic model was proposed and this is explained below. The difference between these models was related to the adsorption term of the reaction rate equations, which will be explained in the corresponding section for each model. The rate and adsorption constants were given by the orthogonalized Arrhenius and Van't Hoff equations, respectively:

$$k'_x = \overline{k'_x} \cdot exp(-Ea_x/R \cdot 1/\theta) \quad (12)$$

$$\overline{k'_x} = k'_{x,\infty} \cdot exp(-Ea_x/R \cdot 1/\overline{T}) \quad (13)$$

$$K_i = \overline{K_i} \cdot exp(-\Delta H_i^0/R \cdot 1/\theta) \quad (14)$$

$$\overline{K_i} = K_{i,\infty} \cdot exp(-\Delta H_i^0/R \cdot 1/\overline{T}) \quad (15)$$

$$1/\theta = 1/T - 1/\overline{T} \quad (16)$$

The equilibrium constants of the reactions involved were estimated using Aspen Hysys:

$$ln\, K_{eqMeOH-CO2} = \frac{6610}{T(K)} - 23.462 \quad (17)$$

$$ln\, K_{eqRWGS} = -4762.4/T(K) + 4.539 \quad (18)$$

$$K_{eqMeOH-CO} = \frac{K_{eqMeOH-CO_2}}{K_{eqRWGS}} \quad (19)$$

The flow of the different species through the catalyst bed was modeled with a pseudohomogeneous, one-dimensional plug flow model, since mass transfer resistance was not observed and a very large reactor L/D ratio was used. In this way, the following expression for the axial flow profiles through the reactor (r_x) for each of the species *i* could be used:

$$r_x = dF_{Pi}/dW \quad (20)$$

where F_{Pi} is the species molar flow and w the catalyst mass. Therefore, the mass balance equations for all the species are given by:

$$dF_{PCO2}/dW = -r_{MeOH-CO2} - r_{RWGS} \quad (21)$$

$$dF_{PH2}/dW = -3 \cdot r_{MeOH-CO2} - r_{RWGS} - 2 \cdot r_{MeOH-CO} \quad (22)$$

$$dF_{PCH3OH}/dW = r_{MeOH-CO2} + r_{MeOH-CO} \quad (23)$$

$$dF_{PCO}/dw = r_{RWGS} - r_{MeOH-CO} \quad (24)$$

$$dF_{PH2O}/dw = r_{MeOH-CO2} + r_{RWGS} \quad (25)$$

The parameter estimation was performed using an iterative nonlinear regression procedure. For given initial parameters, the Matlab subroutine *ode15s* was used to solve the system of ordinary differential equations. The optimum kinetic parameters were then determined by

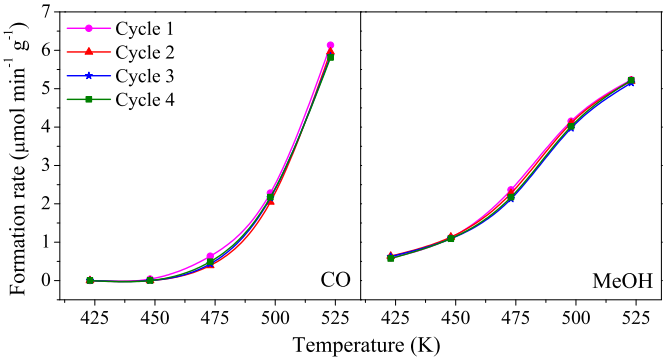

Fig. 3. Stability test with four reaction cycles from 423 to 523 K.

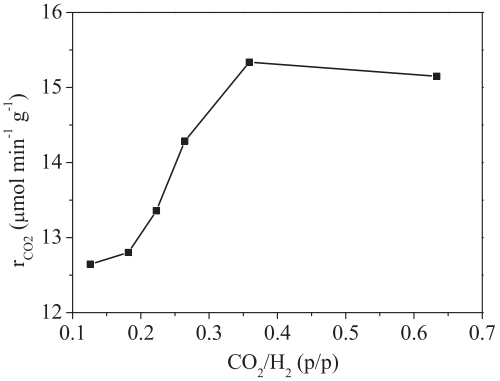

Fig. 4. Influence of the CO_2/H_2 ratio on the CO_2 reaction rate.

Table 2
Reaction mechanism of the CO_2 hydrogenation [10].

Species adsorption
$CO_2 + s_1 \leftrightarrows CO_2{\cdot}s_1$ / $CO_2 + s_3 \leftrightarrows CO_2{\cdot}s_3$
$H_2 + 2\,s_2 \leftrightarrows 2H{\cdot}s_2$
$CH_3OH{\cdot}s_1 \leftrightarrows CH_3OH + s_1$
$CO{\cdot}s_3 \leftrightarrows CO + s_3$ / $CO + s_1 \leftrightarrows CO{\cdot}s_1$
$H_2O{\cdot}s_2 \leftrightarrows H_2O + s_2$
MeOH synthesis from CO_2 hydrogenation (MeOH-CO_2)
$CO_2{\cdot}s_1 + H{\cdot}s_2 \leftrightarrows HCO_2{\cdot}s_1 + s_2$
$HCO_2{\cdot}s_1 + H{\cdot}s_2 \leftrightarrows H_2CO_2{\cdot}s_1 + s_2$ *(r.d.s.)*
$H_2CO_2{\cdot}s_1 + H{\cdot}s_2 \leftrightarrows H_3CO_2{\cdot}s_1 + s_2$
$H_3CO_2{\cdot}s_1 + H{\cdot}s_2 \leftrightarrows H_2CO{\cdot}s_1 + H_2O{\cdot}s_2$
$H_2CO{\cdot}s_1 + H{\cdot}s_2 \leftrightarrows H_3CO{\cdot}s_1 + s_2$
$H_3CO{\cdot}s_1 + H{\cdot}s_2 \leftrightarrows CH_3OH{\cdot}s_1 + s_2$
Reverse Water-Gas-Shift (RWGS)
$CO_2{\cdot}s_3 + H{\cdot}s_2 \leftrightarrows HCO_2{\cdot}s_3 + s_2$ ***(r.d.s.)***
$HCO_2{\cdot}s_3 + H{\cdot}s_2 \leftrightarrows CO{\cdot}s_3 + H_2O{\cdot}s_2$
MeOH synthesis from CO hydrogenation (MeOH-CO)
$CO{\cdot}s_1 + H{\cdot}s_2 \leftrightarrows HCO{\cdot}s_1 + s_2$
$HCO{\cdot}s_1 + H{\cdot}s_2 \leftrightarrows H_2CO{\cdot}s_1 + s_2$
$H_2CO{\cdot}s_1 + H{\cdot}s_2 \leftrightarrows H_3CO{\cdot}s_1 + s_2$
$H_3CO{\cdot}s_1 + H{\cdot}s_2 \leftrightarrows CH_3OH{\cdot}s_1 + s_2$ ***(r.d.s.)***

minimizing the objective function, using the Matlab subroutine *lsqnonlin* (Levenberg–Marquardt). The Weighted Residual Sum of Squares (WRSS) between the theoretical and the experimental partial pressure data was set as the objective function to be minimized:

$$WRSS = \sum_{i=1}^{Nspecies} w_i \cdot \sum_{j=1}^{Ndata} (P_{i,j,exp} - P_{i,j,theo})^2 \tag{26}$$

The weighting factor of each component was calculated by the inverse of their corresponding residuals (s_i^2):

$$w_i = 1/\sqrt{s_i^2/(n-p)} \tag{27}$$

where n and p are the number of data and parameters, respectively. The weighting factors were also calculated using an iterative procedure. A first estimation of the parameters was performed using $w_i = 1$. The corresponding w_i were then calculated and used for the next parameter estimation. This procedure was repeated until significant changes in any of the w_i values were not observed. All kinetic models were subjected to a rigorous statistical analysis. Firstly, the quality of the fit was evaluated by calculating the regression coefficient:

$$r^2 = \frac{\sum_{j=1}^{Ndata} (P_{j,exp} - \overline{P_{exp}})^2 - \sum_{j=1}^{Ndata} \left(P_{j,exp} - P_{j,theo} \right)^2}{\sum_{j=1}^{Ndata} (P_{j,exp} - \overline{P_{exp}})^2} \tag{28}$$

The statistical significance of the parameters was then evaluated using the *t*-test, by the procedure described previously [23], with a confidence interval (α) of 95%. Finally, due to the potential correlation

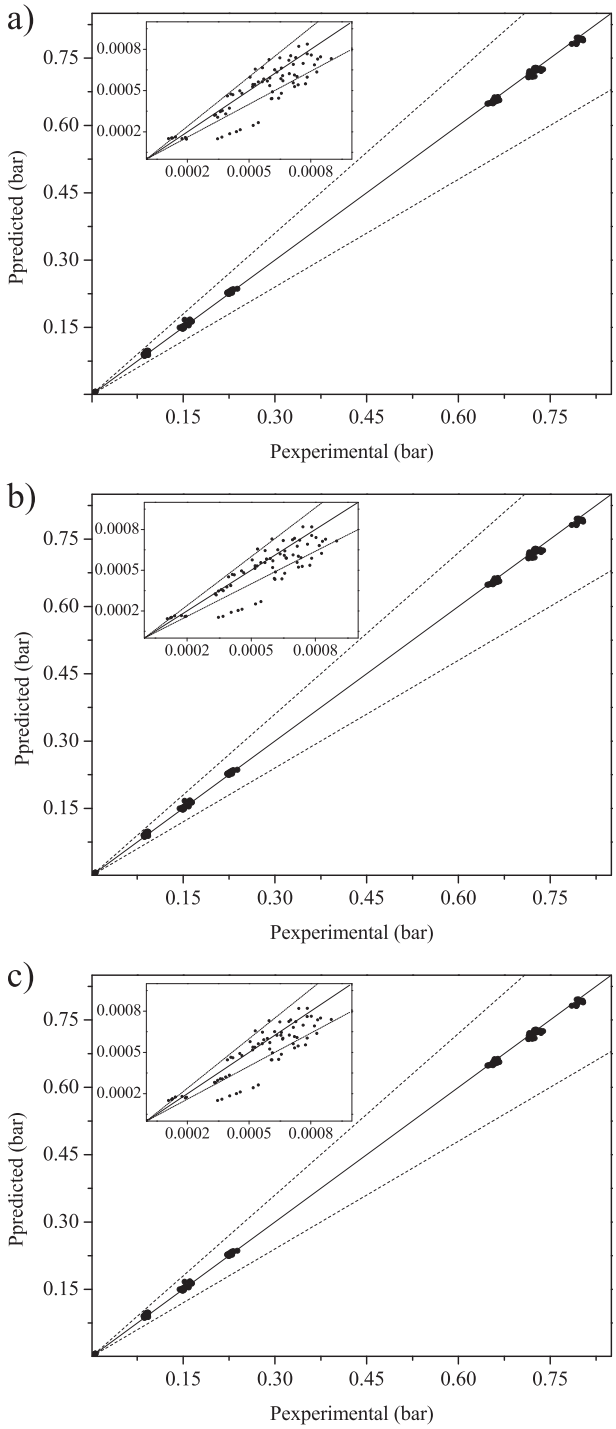

Fig. 5. Parity plot of a) competitive adsorption b) two-site mechanism and c) three site mechanism.

issues related to Langmuir–Hinshelwood models, the correlation matrix p_{ij} was evaluated in each kinetic model. The results obtained in all kinetic models (not shown) revealed that there were no correlation issues.

3.2.3. Model 1: competitive adsorption

Preliminary results revealed that, on the one hand, the adsorption constants of MeOH, CO and H_2O were negligible because of the low concentration of these species in all experiments. Although CO adsorption was expected to affect the kinetic model (as observed experimentally), initial attempts to calculate its adsorption constants (K_{CO} and ΔH_{CO}) led to unusual values, which indeed did not meet the associated

Table 3
Parameter estimation results.

Parameter	Competitive adsorption		Two-sites		Three-sites	
	Value	*t*-Test	Value	*t*-Test	Value	*t*-Test
$\ln(\overline{k'_{MeOH}} + \overline{K_{CO2,s1}} + \overline{K_{H2,s2}})$	−2.79 ± 0.07	42.79	−3.12 ± 0.06	53.00	−3.08 ± 0.15	20.90
$(Ea_{MeOH} + \Delta H_{CO2,s1} + \Delta H_{H2,s2}/(R\cdot\overline{T})$	−0.72 ± 0.05	14.03	−1.20 ± 0.29	4.19	−0.61 ± 0.08	7.71
$\ln(\overline{k'_{RWGS}} + \overline{K_{CO2,s3}} + 0.5\cdot\overline{K_{H2}})$	−3.26 ± 0.04	86.20	−3.57 ± 0.05	65.97	−3.69 ± 0.07	50.03
$(Ea_{RWGS} + \Delta H_{CO2,s1} + 0.5\cdot\Delta H_{H2,s2}/(R\cdot\overline{T})$	8.46 ± 0.39	21.69	9.08 ± 0.51	17.72	10.63 ± 0.84	12.69
$\ln(\overline{K_{CO2,s1}})$	1.98 ± 0.07	28.76	2.91 ± 0.08	35.08	2.96 ± 0.23	13.03
$\Delta H_{CO2,s1}/(R\cdot\overline{T})$	−12.69 ± 0.67	18.85	−14.08 ± 0.66	21.44	−18.18 ± 2.29	7.94
$\ln(0.5\cdot\overline{K_{H2,s2}})$	−0.22 ± 0.04	5.46	−0.46 ± 0.02	18.71	−0.45 ± 0.09	5.22
$0.5\cdot\Delta H_{H2,s2}/(R\cdot\overline{T})$	−7.85 ± 0.39	20.18	−8.47 ± 0.95	8.96	−5.28 ± 0.69	7.60
$\ln(\overline{K_{CO2,s3}})$	$= \ln(\overline{K_{CO2,1}})$	–	$= \ln(\overline{K_{CO2,1}})$	–	2.72 ± 0.15	18.28
$\Delta H_{CO2,s3}/(R\cdot\overline{T})$	$= \Delta H_{CO2,1}/(R\cdot\overline{T})$	–	$= \Delta H_{CO2,1}/(R\cdot\overline{T})$	–	−13.16 ± 1.70	7.76

Table 4
Model discrimination parameters.

Kinetic model	r^2 (Eq. (28))	$(P_{i,j,exp} - P_{i,j,theo})^2$	Hydrogen: parameter constrain (Eq. (35))	
			$-\Delta S_{ads}{}^0/R$	$S_{gas}{}^0/R$
Competitive adsorption	0.9998	0.003488	16.13	15.72
Two-sites	0.9998	0.003486	17.86	15.72
Three-sites	0.9998	0.003475	11.46	15.72

constraints ($K_i > 0$ and $\Delta H_i < 0$). On the other hand, the kinetic parameters for the synthesis of MeOH from CO (Eq. (8)) were also negligible because of the very low concentration of CO, as mentioned above, and this reaction was therefore not considered. It is important to note that this behavior was also observed for the other two kinetic models, so that neither the adsorption of the species mentioned above nor MeOH from CO hydrogenation were considered.

In this model, the catalyst was supposed to have one type of active site and, as a consequence, the species involved in the process were supposed to adsorb competitively on these sites. The model proposed by Skrzypek et al. [10] is the best example in the literature in this respect. Therefore, the adsorption terms could be written as follows according to the preliminary observations:

$$D_{MeOH-CO2} = D_{RWGS} = D_x \quad (29)$$

$$s_1 = s_2 = s_3 = s \quad (30)$$

$$D_x = (1 + K_{CO2,s}\cdot P_{CO2} + \sqrt{K_{H2,s}\cdot P_{H2}})^2 \quad (31)$$

In this model, 8 parameters [2 kinetic constants at the reference temperature (225 °C), 2 activation energies, 2 adsorption constants at the reference temperature and 2 adsorption enthalpies] were estimated. The parity plot for the prediction of the species partial pressures is shown in Fig. 5a. The parameter estimation results are listed in Table 3 along with the corresponding *t*-test values.

3.2.4. Model 2: two-site mechanism

Most of the kinetic models for MeOH synthesis reported in the literature using Cu/ZnO-based catalysts [11,13,24] concern the two-site adsorption mechanism. In this respect, ZnO was believed to adsorb H_2 and H_2O, whereas carbonaceous species were adsorbed on Cu. In this study, a similar two-site adsorption mechanism was proposed and the adsorption terms are as follows:

$$D_{MeOH-CO2} = D_{RWGS} = D_x \quad (32)$$

$$s_1 = s_3 = s \quad (33)$$

$$D_x = (1 + K_{CO2,s}\cdot P_{CO2})\cdot(1 + \sqrt{K_{H2,s2}\cdot P_{H2}}) \quad (34)$$

As in the previous model, 8 parameters were estimated in this model. The corresponding parity plot is shown in Fig. 5b and the parameter estimation results are listed in Table 3.

3.2.5. Model 3: three-site mechanism

In previous work by our group [15] it was concluded that the Pd-Cu-Zn catalyst, which showed the best results, had three different active sites: PdZn alloy, on which MeOH synthesis from CO_2 hydrogenation occurred, PdCu alloy, which was prone to catalyze the RWGS reaction, and ZnO sites, which are involved in both reactions. In line with this conclusion, a three-site adsorption mechanism was proposed in this work and it was considered that carbonaceous molecules (in this case CO_2) adsorbed differently on PdZn or PdCu, whereas ZnO interacted with H_2. Therefore, the adsorption terms for this model can be written

Table 5
Kinetic parameters of three-sites model and comparison with the literature.

Parameter	This work	Graaf (1988)	Skrzypek (1991)	Park (2014)	Units
k'_{MeOH} (498 K)	$4.0\cdot10^{-4}$	$6.3\cdot10^{-5}$[a]	$8.7\cdot10^{-3}$	$4.9\cdot10^{-3}$[c]	$mol\cdot kg^{-1}\cdot s^{-1}$
Ea_{MeOH}	116.5	65.2	104.7	68.3	$kJ\cdot mol^{-1}$
k'_{RWGS} (498 K)	$1.4\cdot10^{-4}$	$8.3\cdot10^{-5}$[a]	$7.2\cdot10^{-3}$	$6.1\cdot10^{-4}$[c]	$mol\cdot kg^{-1}\cdot s^{-1}$
Ea_{RWGS}	120.4	123.4	104.7	126.6	$kJ\cdot mol^{-1}$
$K_{CO2,\ s1}$ (498 K)	19.2	1.2	0.4	–	bar^{-1}
$\Delta H_{CO2,\ s1}$	−75.3	−67.4	−75.4	–	$kJ\cdot mol^{-1}$
$K_{H2,\ s2}$ (498 K)	0.4	3.8[b]	0.1	–	bar^{-1}
$\Delta H_{H2,\ s2}$	−43.7	−104.5[b]	−75.4	–	$kJ\cdot mol^{-1}$
$K_{CO2,\ s3}$ (498 K)	15.2	–	–	–	bar^{-1}
$\Delta H_{CO2,\ s3}$	−54.5	–	–	–	$kJ\cdot mol^{-1}$

[a] $[k'_{MeOH}$ (498 K)]: $mol\cdot s^{-1}\cdot kg^{-1}\cdot bar^{-1}$, $[k'_{RWGS}$ (498 K)]: $mol\cdot s^{-1}\cdot kg^{-1}\cdot bar^{-1/2}$.
[b] Refers to $H_2O/H_2{}^{1/2}$.
[c] $[k'_{MeOH}$ (498 K)]: $mol\cdot s^{-1}\cdot kg^{-1}\cdot bar^{-1.5}$, $[k'_{RWGS}$ (498 K)]: $mol\cdot s^{-1}\cdot kg^{-1}\cdot bar^{-1}$.

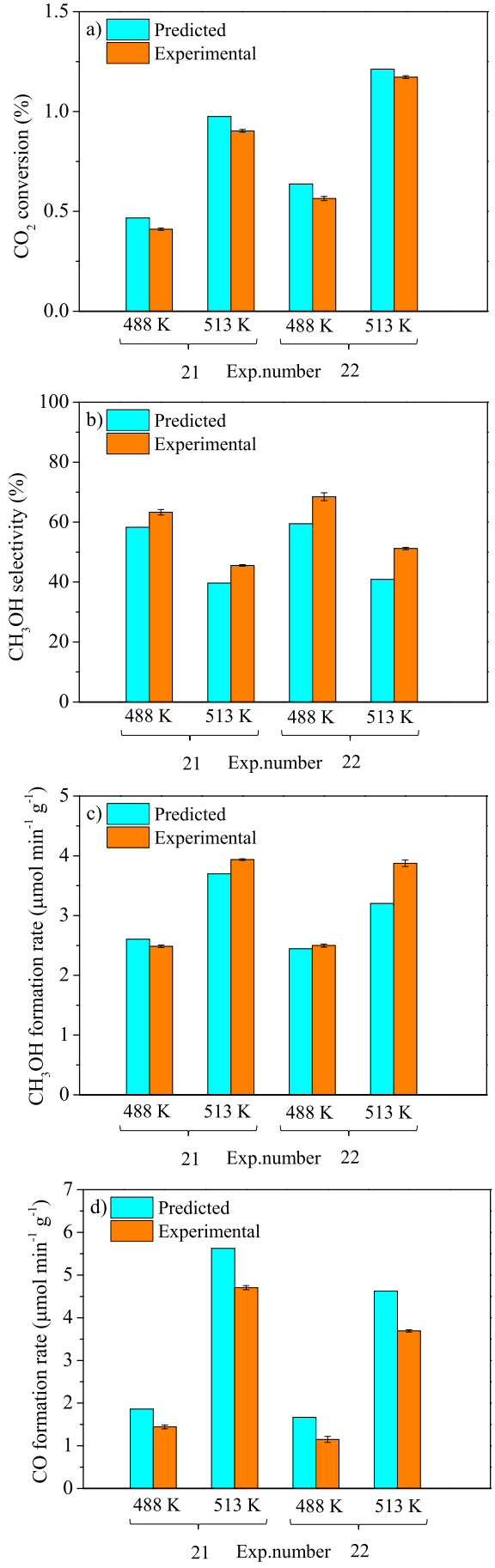

Fig. 6. Comparison between experimental and predicted catalytic results in a) CO_2 conversion, b) CH_3OH selectivity, c) CH_3OH formation rate and d) CO formation rate.

as follows:

$$D_{MeOH-CO2} = (1 + K_{CO2,s1}\cdot P_{CO2})\cdot(1 + \sqrt{K_{H2,s2}\cdot P_{H2}}) \quad (35)$$

$$D_{RWGS} = (1 + K_{CO2,s3}\cdot P_{CO2})\cdot(1 + \sqrt{K_{H2,s2}\cdot P_{H2}}) \quad (36)$$

In this model there were three adsorption species (CO_2 at two sites and H_2) and therefore 10 parameters were estimated. The corresponding parity plot is depicted in Fig. 5c and the parameter estimation results are listed in Table 3.

4. Discussion

It can be observed from the results in Table 3 that all kinetic models were developed using lumped parameters, with the aim of minimizing the potential correlation issues associated with the proposed equations (for example, the use of the full Arrhenius and Van't Hoff equations). The results of the *t*-test revealed that all parameters were statistically meaningful, as all t values were higher than the corresponding threshold (1.96, see Table 3). This fact – together with the lack of difference between the parity plots (Fig. 5) – made it difficult at first glance to carry out the model discrimination.

As a consequence of the above, the kinetic model results should be compared in more detail. The variables that were compared to select the best kinetic model are listed in Table 4. If we consider the first column, it can be seen that the regression coefficient for all models (r^2, Eq. (28)) was 0.9998, which confirmed (i) that all of the models predicted the experimental results well and (ii) that it was not possible to discriminate any model according to this variable. The unweighted residual sum of squares showed slight differences between the proposed kinetic models. In this regard, the three-site model led to the lowest value, which confirmed that this model predicted the experimental results better than the other ones. It is important to note that the *WRSS* values (Eq. (26)) could not be used to compare the kinetic models since the weighting factors were not the same in each case.

Finally, as proposed by Graaf et al. [11], the kinetic parameters should meet the following constraints: $k_x > 0$, $Ea_x > 0$, $K_i > 0$, $\Delta H^{\circ}_i < 0$, and the following one, which is included in Table 4:

$$0 < -\Delta S^0_{ads}/R < S^0_{gas}/R \quad (37)$$

where

$$K = \exp(-\Delta S^0_{ads}/R)\cdot\exp(-\Delta H^0_{ads}/R\cdot T) \quad (38)$$

It can be seen from the results in Table 4 that the corresponding H_2 parameter only meets this constraint in the three-site kinetic model (CO_2 parameters meet it in all models). On considering these findings, the three-site kinetic model was chosen as the one that provided the best prediction of the experimental results, since it provides the least unweighted residual sum of squares and all of its parameters satisfied their corresponding constraints.

Once the model discrimination had been performed, the kinetic parameters were calculated from the corresponding lumped ones (Table 5). These values were also compared with those of some other models reported in the literature. It is important to note that, since each model was developed for different mechanisms, reaction conditions and catalysts, it was practically impossible to make direct comparisons, especially in terms of kinetic and adsorption constants. However, comparison of the activation energies and adsorption enthalpies was easier. On the one hand, the Ea_{MeOH} in this work was higher than those reported in the literature, especially when compared to the values of Graaf [11] and Park [12], whereas all Ea_{RWGS} values were similar. The ΔH_{CO2} values were all similar to each other. Generally, the estimated parameters obtained in this work were of the same order of magnitude

as those reported in the literature.

Finally, the quality of the model was checked by using it to predict the species partial pressures under different experimental conditions that were not used in the parameter fitting procedure. These predicted values are shown in Fig. 6 along with the experimental values for the sake of comparison. It was observed that the proposed kinetic model predicted the experimental results well and the only significant deviations were observed in the CO counterparts.

5. Conclusions

The following conclusions can be drawn from the work described above:

- The sensitivity study revealed that there was a temperature at which the maximum MeOH formation rate was attained and this is due to the exothermic nature of the reaction. Moreover, higher MeOH selectivity was obtained when the CO_2/H_2 ratio was lower. Finally, the presence of MeOH or CO in the feed stream did not have an appreciable effect on the catalytic performance beyond shifting the corresponding reaction equilibria.
- A proper kinetic analysis of the CO_2 hydrogenation to MeOH was carried out. Three Langmuir–Hinshelwood (LH) kinetic models, in which the nature of the active sites was varied, were successfully proposed.
- All kinetic models predicted the experimental results well and were statistically meaningful. Among them, the three-site LH kinetic model provided the least unweighted residual sum of squares and met all the established constraints. As a consequence, this was selected as the best kinetic model.
- This model provided a good prediction of the experimental results obtained in extra experiments that were carried out under different conditions.
- The kinetic model proposed in this work is consistent with the catalytic observations reported previously.

Acknowledgements

The authors would like to thank the Ministerio de Economía y Competitividad (Project No. PCIN-2013-183), the Spanish government (grant FPU13/00727) and the University of Castilla – La Mancha (Energy and environment talent program – E2TP) for their financial support.

References

[1] F.A. Rahman, M.M.A. Aziz, R. Saidur, W.A.W.A. Bakar, M.R. Hainin, R. Putrajaya, N.A. Hassan, Pollution to solution: capture and sequestration of carbon dioxide (CO_2) and its utilization as a renewable energy source for a sustainable future, Renew. Sust. Energ. Rev. 71 (2017) 112–126.

[2] S. Saeidi, N.A.S. Amin, M.R. Rahimpour, Hydrogenation of CO_2 to value-added products - a review and potential future developments, J. CO_2 Util. 5 (2014) 66–81.

[3] S.G. Jadhav, P.D. Vaidya, B.M. Bhanage, J.B. Joshi, Catalytic carbon dioxide hydrogenation to methanol: a review of recent studies, Chem. Eng. Res. Des. 92 (2014) 2557–2567.

[4] N.A. Karim, S.K. Kamarudin, K.S. Loh, Performance of a novel non-platinum cathode catalyst for direct methanol fuel cells, Energy Convers. Manag. 145 (2017) 293–307.

[5] G.A. Olah, Beyond oil and gas: the methanol economy, Angew. Chem. Int. Ed. 44 (2005) 2636–2639.

[6] W. Wisaijorn, Y.P. Arporn, P. Marin, S. Ordóñez, S. Assabumrungrat, P. Praserthdam, D. Saebea, S. Soisuwan, Reduction of carbon dioxide via catalytic hydrogenation over copper-based catalysts modified by oyster shell-derived calcium oxide, J. Environ. Chem. Eng. 5 (2017) 3115–3121.

[7] F. Zhao, M. Gong, K. Cao, Y. Zhang, J. Li, R. Chen, Atomic layer deposition of Ni on Cu nanoparticles for methanol synthesis from CO_2 hydrogenation, ChemCatChem 9 (2017) 3772–3778.

[8] B. An, J. Zhang, K. Cheng, P. Ji, C. Wang, W. Lin, Confinement of Ultrasmall Cu/ZnO_x Nanoparticles in Metal-organic Frameworks for Selective Methanol Synthesis From Catalytic Hydrogenation of CO_2, 139 (2017), pp. 3834–3840.

[10] J. Skrzypek, M. Lachowska, H. Moroz, Kinetics of methanol synthesis over commercial copper/zinc oxide/alumina catalysts, Chem. Eng. Sci. 46 (1991) 2809–2813.

[11] G.H. Graaf, E.J. Stamhuis, A.A.C.M. Beenackers, Kinetics of low-pressure methanol synthesis, Chem. Eng. Sci. 43 (1988) 3185–3195.

[12] N. Park, M.J. Park, Y.J. Lee, K.S. Ha, K.W. Jun, Kinetic modeling of methanol synthesis over commercial catalysts based on three-site adsorption, Fuel Process. Technol. 125 (2014) 139–147.

[13] H.W. Lim, M.J. Park, S.H. Kang, H.J. Chae, J.W. Bae, K.W. Jun, Modeling of the kinetics for methanol synthesis using Cu/ZnO/Al $_2O_3$/ZrO_2 catalyst: influence of carbon dioxide during hydrogenation, Ind. Eng. Chem. Res. 48 (2009) 10448–10455.

[14] D.L. Chiavassa, S.E. Collins, A.L. Bonivardi, M.A. Baltanás, Methanol synthesis from CO_2/H_2 using Ga_2O_3-Pd/silica catalysts: kinetic modeling, Chem. Eng. J. 150 (2009) 204–212.

[15] J. Díez-Ramírez, J.A. Díaz, P. Sánchez, F. Dorado, Optimization of the Pd/Cu ratio in Pd-Cu-Zn/SiC catalysts for the CO_2 hydrogenation to methanol at atmospheric pressure, J. CO_2 Util. 22 (2017) 71–80.

[16] J. Díez-Ramírez, P. Sánchez, J.L. Valverde, F. Dorado, Electrochemical promotion and characterization of PdZn alloy catalysts with K and Na ionic conductors for pure gaseous CO_2 hydrogenation, J. CO_2 Util. 16 (2016) 375–383.

[17] Y. Choi, K. Futagami, T. Fujitani, J. Nakamura, The difference in the active sites for CO_2 and CO hydrogenations on Cu/ZnO-based methanol synthesis catalysts, Catal. Lett. 73 (2001) 27–31.

[18] T. Fujitani, M. Saito, Y. Kanai, T. Kakumoto, T. Watanabe, J. Nakamura, T. Uchijima, The role of metal oxides in promoting a copper catalyst for methanol synthesis, Catal. Lett. 25 (1994) 271–276.

[19] O.S. Joo, K.D. Jung, S.H. Han, S.J. Uhm, D.K. Lee, S.K. Ihm, Migration and reduction of formate to form methanol on Cu/ZnO catalysts, Appl. Catal. A Gen. 135 (1996) 273–286.

[20] G.F. Froment, K.B. Bischoff, J. De Wilde, Chemical Reactor Analysis and Design, Wiley, New York, 1990.

[21] Chapter 9, Heterogeneous catalysis, Comprehensive Chemical Kinetics, 40 2004, pp. 273–308.

[22] E.L. Kunkes, F. Studt, F. Abild-Pedersen, R. Schlögl, M. Behrens, Hydrogenation of CO_2 to methanol and CO on Cu/ZnO/Al_2O_3: is there a common intermediate or not? J. Catal. 328 (2015) 43–48.

[23] J.M. García-Vargas, J.L. Valverde, J. Díez, F. Dorado, P. Sánchez, Catalytic and kinetic analysis of the methane tri-reforming over a Ni-Mg/β-SiC catalyst, Int. J. Hydrog. Energy 40 (2015) 8677–8687.

[24] M. Peter, M.B. Fichtl, H. Ruland, S. Kaluza, M. Muhler, O. Hinrichsen, Detailed kinetic modeling of methanol synthesis over a ternary copper catalyst, Chem. Eng. J. 203 (2012) 480–491.